

## Three-dimensional (3D) slope stability analysis using stability charts

Arunav Chakraborty & Diganta Goswami

To cite this article: Arunav Chakraborty & Diganta Goswami (2018): Three-dimensional (3D) slope stability analysis using stability charts, International Journal of Geotechnical Engineering, DOI: [10.1080/19386362.2018.1465743](https://doi.org/10.1080/19386362.2018.1465743)

To link to this article: <https://doi.org/10.1080/19386362.2018.1465743>



Published online: 02 May 2018.



Submit your article to this journal [↗](#)



View related articles [↗](#)



View Crossmark data [↗](#)



## Three-dimensional (3D) slope stability analysis using stability charts

Arunav Chakraborty<sup>a</sup> and Diganta Goswami<sup>b</sup>

<sup>a</sup>Civil Engineering Department, Tezpur University, Tezpur, India; <sup>b</sup>Civil Engineering Department, Assam Engineering College, Jalukbari, India

### ABSTRACT

Stability of slopes is a very serious issue in the field of geotechnical engineering. The analysis and design of failing slopes requires a thorough knowledge of the failure mechanism in order to choose the right slope stability analysis method. The two-dimensional (2D) slope stability methods are very common to the engineers because of the simplicity in their assumptions. As a result the analysis results vary greatly between the different analysis methods. The importance of three-dimensional (3D) slope stability analysis greatly increased where the geometry of the problem becomes complex which makes it very difficult to solve using 2D analysis. A lot many 2D slope stability methods were extended to 3D methods since 1970s based on limit equilibrium (LE) and finite element approaches. In this paper, slopes were analysed using 3D limit equilibrium method (LEM) using SLIDE3 software having different geometry and soil parameters and finally stability charts were prepared to calculate the FOS of the slopes. It is found that the slope stability factor can be read from the stability charts without the need for iterations.

### ARTICLE HISTORY

Received 27 February 2018  
Accepted 9 April 2018

### KEYWORDS

Slope stability; Geotechnical Engineering; failure mechanism; limit equilibrium method

### Introduction

Three-dimensional (3D) slope stability problems are very rarely used in practice because of higher complicacy compared to two-dimensional (2D) methods. 2D LE methods are based on plane strain conditions that assumes the slide mass or cross-section do not change in the direction perpendicular to the slide movement, and therefore, the 3D effects are neglected. This assumption is acceptable if the ratio of width (B) to the height (H) of the slope is greater than four. However, in most of the cases, the width to height ratio is not sufficiently long and varies perpendicular to the slide movement. Therefore, the application of 2D analyses to 3D problem is not accurate but believed to be conformist from the engineering perspective because the end effects are neglected. Hence, a 2D (plane strain) analysis can be regarded as conservative where 3D failure is expected to occur and it is often preferred in the design (Cornforth 2005). The importance of 3D analysis grows significantly where the nature of the slope is highly complex and it is difficult to select a 2D plane strain analysis. Fredlund and Krahn in 1978 illustrated the benefits associated with performing 3D slope stability. In the recent past, many 3D slope stability methods were developed ranging from method of columns based on variational calculus to the use of dynamic programming. The increase in the importance of 3D slope stability is due to the fact that most of the slope failures are three-dimensional in nature having a dish-shaped failure surface. Like the 2D methods, the 3D methods also require some assumptions to achieve a statically determinate definition of the problem. Some 3D methods do it by decreasing the number of unknowns, while some others achieve it by increasing the number of equations or both, such that the two numbers tally with each other.

An extensive literature review regarding stability analysis of slopes was presented by Duncan in 1996. Some of the other newer literature surveys focusing particularly on 3D slope stability analysis can be found in more recent articles by Griffiths and Marquez (2007) and Chakraborty and Goswami (2016). The first 3D slope stability method was developed by Anagnosti (1969) by extending the earlier Morgenstern and Price (M-P) method (1965). A similar technique was followed by other researchers (Hungar (1987), Ugai (1988), Hungar, Salgado, and Byrne (1989), Cheng and Yip (2007) and Sun, Zheng, and Jiang (2011)) to develop 3D methods from the existing 2D Limit equilibrium methods (LEMs). The assumptions of each of the 3D methods developed followed the same assumptions of 2D methods. However, the slip surface was assumed different for different slopes. Some researchers assumed it to be a spoon-shaped or circular cross-section while others assumed it to be a horn shaped or cylindrical cross-section.

In the limit analysis of 2D slope collapse, it is the rotational mechanism that leads to the most critical cases (Chen 1975). Here, slopes were analysed using 3D limit equilibrium method having different geometry and soil parameters with the inclusion of pore water pressure and finally stability charts were prepared. These charts allow calculation of the FOS of the slopes against a 3D failure without the need for an iterative procedure.

### 3D numerical method

A 3D numerical method is developed based on the extension of 2D Bishop's simplified method. The slip surface for this analysis is assumed to be spherical in both y-direction and z-direction. The whole slip surface has been discretized into a number of

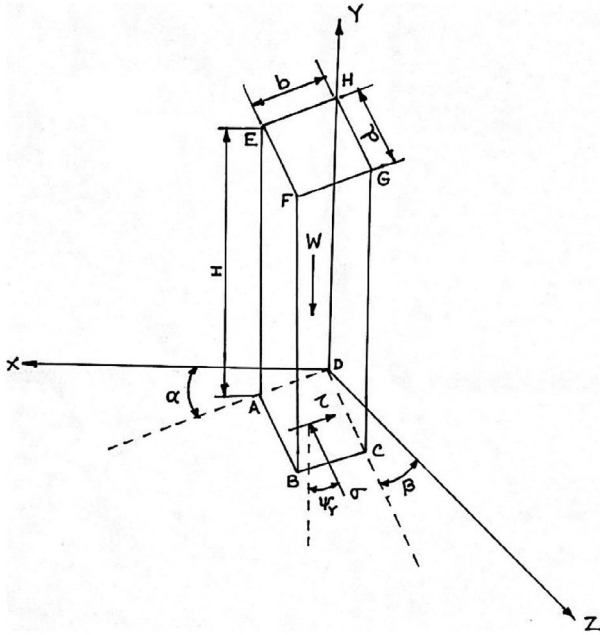


Figure 1. Forces acting on a single column.

columns. To make the problem statically determinate, the vertical shear forces acting on both the longitudinal and lateral vertical faces are neglected as shown in Figure 1.

From Force Equilibrium Equation,  
 $\Sigma V = 0$

$$W - \sigma \cos \psi_y - \tau \sin \alpha = 0 \quad (1)$$

$$W = \sigma \cos \psi_y + \tau \sin \alpha \quad (2)$$

We know that

$$\tau = \frac{CA + (\sigma - uA) \tan \varphi}{F} \quad (3)$$

Putting the value of  $\tau$  in (2)

$$W = \sigma \cos \psi_y + \left\{ \frac{CA + (\sigma - uA) \tan \varphi}{F} \right\} \sin \alpha \quad (4)$$

$$W = \sigma \cos \psi_y + \frac{CA}{F} \sin \alpha + \frac{(\sigma - uA) \tan \varphi \sin \alpha}{F} \quad (5)$$

$$W = \sigma \cos \psi_y + \frac{CA}{F} \sin \alpha + \frac{\sigma \tan \varphi \sin \alpha}{F} - \frac{uA \tan \varphi \sin \alpha}{F} \quad (6)$$

$$W = \sigma \left( \cos \psi_y + \frac{\tan \varphi \sin \alpha}{F} \right) + \frac{CA}{F} \sin \alpha - \frac{uA \tan \varphi \sin \alpha}{F} \quad (7)$$

$$\sigma \left( \cos \psi_y + \frac{\tan \varphi \sin \alpha}{F} \right) = W - \frac{CA}{F} \sin \alpha + \frac{uA \tan \varphi \sin \alpha}{F} \quad (8)$$

$$\sigma = \frac{W - \frac{CA}{F} \sin \alpha + \frac{uA \tan \varphi \sin \alpha}{F}}{\cos \psi_y + \frac{\tan \varphi \sin \alpha}{F}} \quad (9)$$

$$\sigma = \frac{W + \frac{1}{F} \sin \alpha (uA \tan \varphi - CA)}{\cos \psi_y + \frac{\tan \varphi \sin \alpha}{F}} \quad (10)$$

where  $W$  is the total weight of the column,  $u$  is the pore water pressure acting in the centre of the column base,  $C$  is the cohesion,  $\varphi$  is the angle of internal friction,  $A$  is the base area and  $F$  is the factor of safety.

Hovland (1977) derived the column base area,  $A$  which is given by

$$A = b.d. \frac{\sqrt{1 - \sin^2 \alpha \sin^2 \beta}}{\cos \alpha \cos \beta} \quad (11)$$

The angle  $\psi_y$  between the direction of the normal force  $\sigma$  and the vertical axis is obtained from the geometry as follows:

$$\psi_y = \cos^{-1} \sqrt{\left( \frac{1}{\tan^2 \alpha + \tan^2 \beta + 1} \right)} \quad (12)$$

Now the whole area of the sliding mass is divided into a number of columns arranged in rows of uniform width as shown in Figure 2.

In general, for an assemblage of  $j$  columns, a moment equilibrium equation can be written as follows:

$$\sum_{i=1}^j (\sigma - uA) \frac{\tan \varphi + CA}{F} = \sum_{i=1}^j W \sin \alpha \quad (13)$$

$$F \left( \sum_{i=1}^j W \sin \alpha \right) = \sum_{i=1}^j (\sigma - uA) \tan \varphi + CA \quad (14)$$

Putting the value of  $\sigma$  from Equation (10)

$$F \left( \sum_{i=1}^j W \sin \alpha \right) = \sum_{i=1}^j \left[ \frac{W + \frac{1}{F} \sin \alpha (uA \tan \varphi - CA)}{\cos \psi_y + \frac{\tan \varphi \sin \alpha}{F}} - uA \right] \tan \varphi + CA \quad (15)$$

$$F \left( \sum_{i=1}^j W \sin \alpha \right) = \sum_{i=1}^j \left[ \frac{W - \frac{CA}{F} \sin \alpha \tan \varphi - \frac{CA}{F} \sin \alpha - uA (\cos \psi_y + \frac{\tan \varphi \sin \alpha}{F})}{\cos \psi_y + \frac{\tan \varphi \sin \alpha}{F}} \right] \tan \varphi + CA \quad (16)$$

$$F \left( \sum_{i=1}^j W \sin \alpha \right) = \sum_{i=1}^j \left( \frac{W - \frac{CA}{F} \sin \alpha - uA \cos \psi_y}{\cos \psi_y + \frac{\tan \varphi \sin \alpha}{F}} \right) \tan \varphi + CA \quad (17)$$

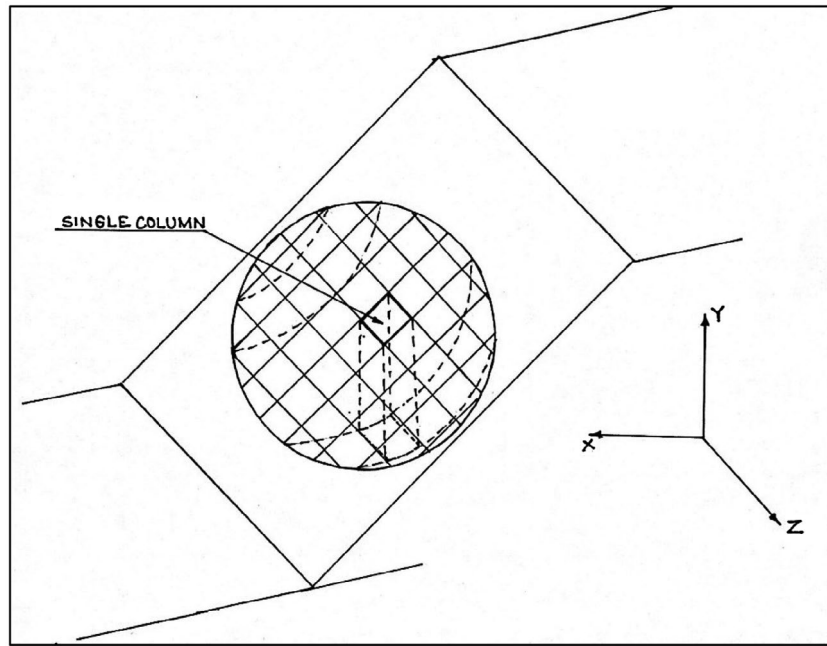


Figure 2. Discretization of a failure mass.

$$F \left( \sum_{i=1}^j W \sin \alpha \right) = \sum_{i=1}^j \left[ \frac{\left( W - \frac{CA}{F} \sin \alpha - uA \cos \psi_y \right) \tan \varphi + CA \left( \cos \psi_y + \frac{\tan \varphi \sin \alpha}{F} \right)}{\cos \psi_y + \frac{\tan \varphi \sin \alpha}{F}} \right] \quad (18)$$

$$F \left( \sum_{i=1}^j W \sin \alpha \right) = \sum_{i=1}^j \left[ \frac{\left( W \tan \varphi - uA \cos \psi_y \tan \varphi \right) + CA \cos \psi_y}{\cos \psi_y + \frac{\tan \varphi \sin \alpha}{F}} \right] \quad (19)$$

$$F \left( \sum_{i=1}^j W \sin \alpha \right) = \sum_{i=1}^j \left[ \frac{\left( W - uA \cos \psi_y \right) \tan \varphi + CA \cos \psi_y}{\cos \psi_y + \frac{\tan \varphi \sin \alpha}{F}} \right] \quad (20)$$

$$F = \frac{\sum_{i=1}^j \left[ \frac{\left( W - uA \cos \psi_y \right) \tan \varphi + CA \cos \psi_y}{\cos \psi_y + \frac{\tan \varphi \sin \alpha}{F}} \right]}{\sum_{i=1}^j W \sin \alpha} \quad (21)$$

The factor of safety can be obtained from Equation (21) when solved by an iterative procedure.

### 3D stability charts

Charts representing the slope stability analyses results require an iterative procedure to arrive at the safety factor. *Taylor's (1937)* stability charts were given in terms of stability factor  $c/\gamma HF$ , where  $c$  is the cohesion intercept needed to maintain limit equilibrium and  $H$  is the height of the slope. The factor  $c/\gamma HF$  is

plotted against slope inclinations  $\beta$  for a variety of friction angle  $\varphi$ . If slope angle  $\beta$  and friction angle  $\varphi$  for a slope is given, one can easily find the value of  $F$  by calculating the value of  $c/\gamma H$  (given slope) from Taylor's Stability Chart. But the safety factor needs to be applied to  $\tan \varphi$  also.

$$F = \frac{c}{c_d} = \frac{\tan \varphi}{\tan \varphi_d} \quad (22)$$

Hence, the process becomes iterative. Taylor's stability chart fails to define the location of the slip circle. This problem was solved by *Baker (2003)* where he proposed design charts that can compute the coordinates, centre and radius of the slip circle. *Steward et al. (2011)* revisited Taylor's stability charts and two modified design charts were presented, one for undrained ( $\varphi_u = 0$ ) clays and other for drained ( $c'-\varphi'$ ) soils. The chart for undrained clays consists of compound circles having two separate arcs connected by a straight line at the interface with the stiff stratum which were not present in Taylor's chart. The chart for drained soils enables to compute the slope safety factor without any iterative procedure. *Michalowski (2002)* produced a set of stability charts for slopes based on the kinematic approach of limit analysis. These charts have the advantage of using them for slopes subjected to pore water pressure and seismic forces. *Michalowski (2010)* extended his 2D work to 3D and presented stability charts which do not require an iterative procedure to arrive at the factor of safety. A 3D rotational failure mechanism constructed by *Michalowski and Drescher (2009)* with the failure surface being a section of a curvilinear cone (horn shaped) was adopted to develop the stability charts.

The work discussed herein required thousands of analyses of slopes on a micro-computer having different geometry and soil parameters. All the analyses were carried out using the numerical method discussed above. The process of iterations will be eliminated if the results are plotted as a function of  $c \cot \varphi$ . This is

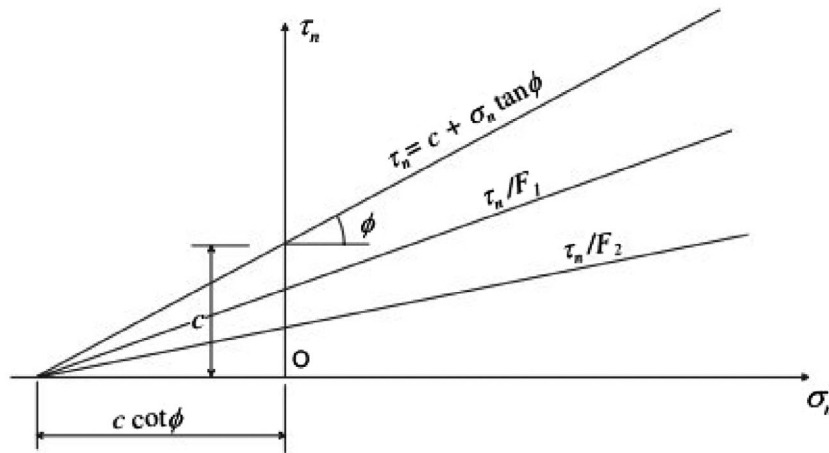


Figure 3. Independence of parameter  $c \cot$  of the safety factor.

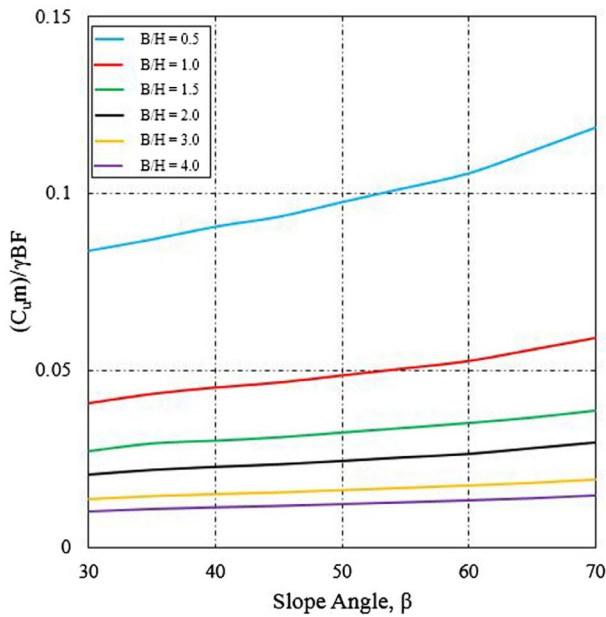


Figure 4. Stability charts for undrained soil.

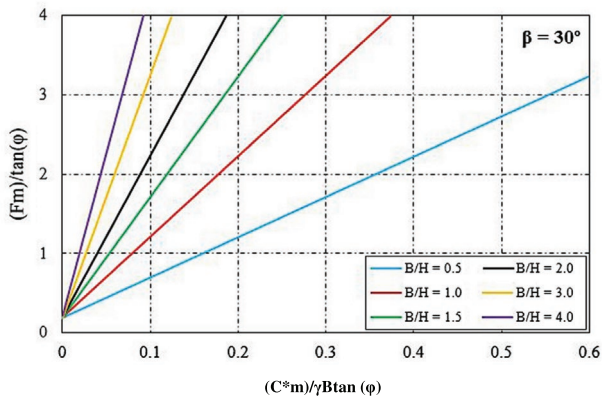


Figure 5. Stability chart for drained soil for slope angle  $30^\circ$ .

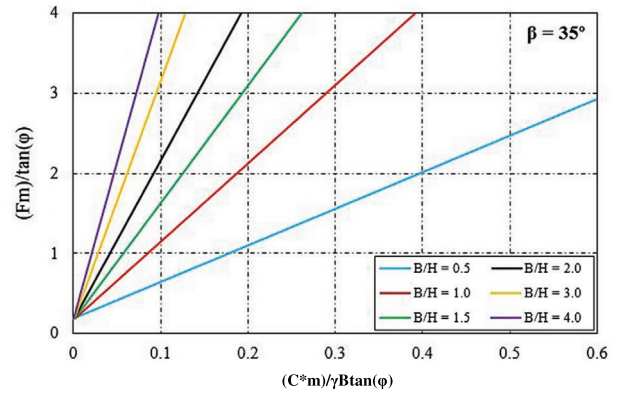


Figure 6. Stability chart for drained soil for slope angle  $35^\circ$ .

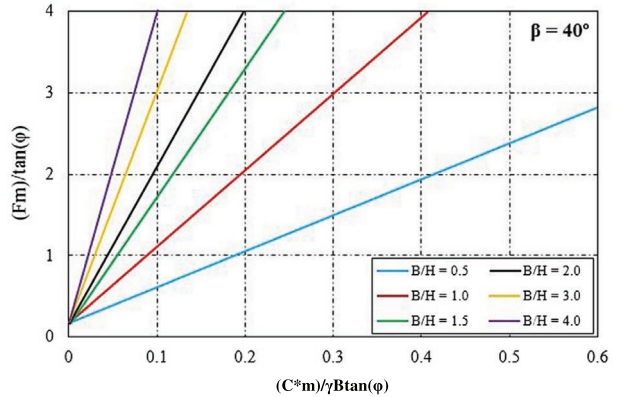


Figure 7. Stability chart for drained soil for slope angle  $40^\circ$ .

obvious that  $c \cot \phi$  is independent of the safety factor as from the definition and illustrated in Figure 3. No matter what the safety factor, product  $c \cot \phi$  will always remain the same. It is hence

necessary to plot the reciprocal of  $\tan \phi$ ,  $F_m/\tan(\phi)$  versus the dimensionless parameter  $C^*m/\gamma B \tan(\phi)$  and produce stability charts for different values of  $B/H$  at different slope inclination. Here,  $c$  is the cohesion intercept,  $H$  is the height of the slope,  $B$  is the width of the slope,  $\gamma$  is the *in situ* unit weight of the soil,  $\phi$  is the angle of internal friction and ' $m$ ' is a dimensionless parameter which is given by ratio of water table depth ( $h$ ) and the height of the slope ( $H$ ). The groundwater head is an alternative quantity for the active pore pressure. The groundwater head is defined as:

$$p = \gamma_w(z - h) \quad (23)$$

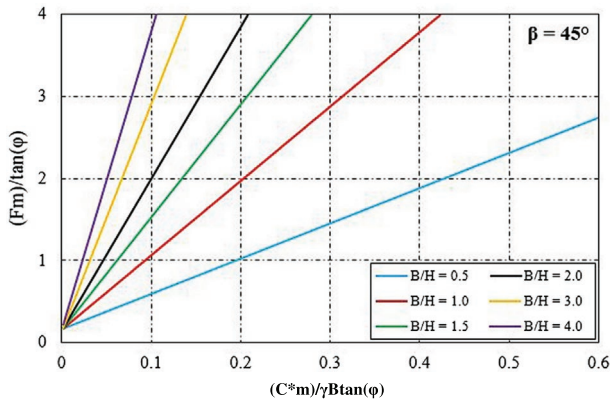


Figure 8. Stability chart for drained soil for slope angle 45°.

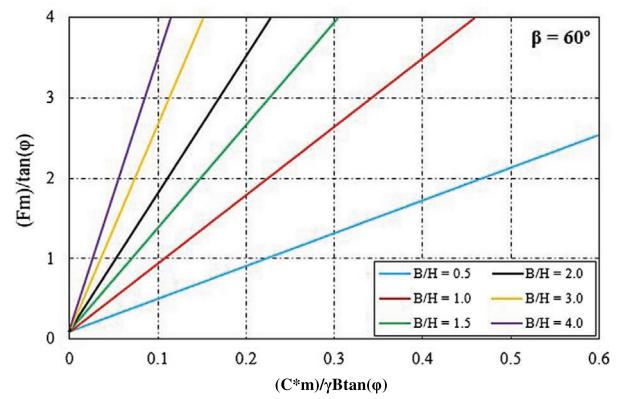


Figure 11. Stability chart for drained soil for slope angle 60°.

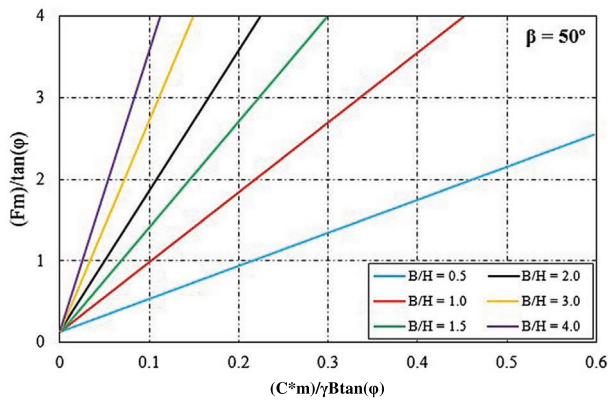


Figure 9. Stability chart for drained soil for slope angle 50°.

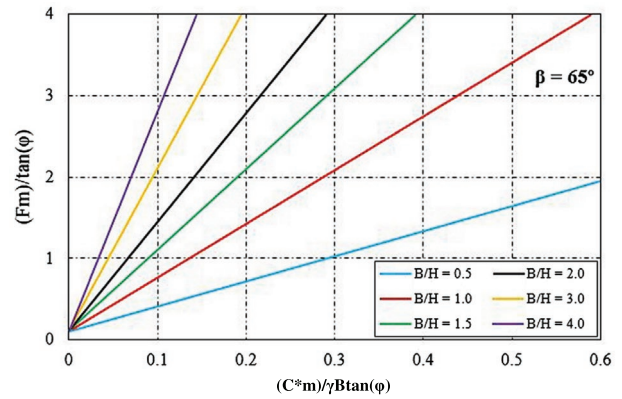


Figure 12. Stability chart for drained soil for slope angle 65°.

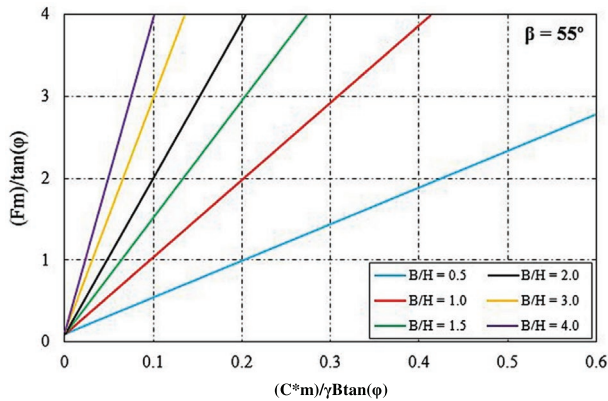


Figure 10. Stability chart for drained soil for slope angle 55°.

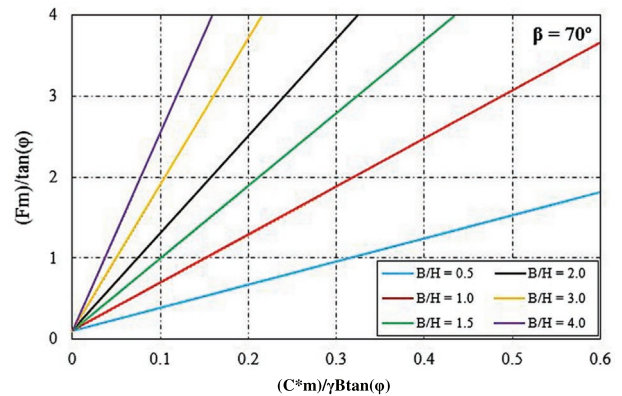


Figure 13. Stability chart for drained soil for slope angle 70°.

where  $h$  is the depth of water table,  $p$  is the active pore pressure (i.e. steady-state pore pressures + excess pore pressures) and  $\gamma_w$  is the unit weight of water.

## Computational results

### Stability charts for undrained soils ( $\varphi_u = 0$ soil)

The computational results are first presented for the undrained failure of the soil ( $\varphi_u = 0$ ) as shown in Figure 4. The

non-dimensional parameter  $(C_u^*m)/\gamma BF$  is presented as a function of slope inclination angle  $\beta$  for different ratios of  $B/H$ . The use of this chart is very straight forward. If the slope geometry and hydrological condition is known, one can easily calculate the value of  $C_u^*m/\gamma BF$  from which the FOS can be found out.

### Stability charts for drained soils ( $c - \varphi$ soil)

The remaining computational results are represented for soil strength characterized by  $c$  and  $\varphi$ . Here, the results are presented as a function of  $F_m/\tan(\varphi)$  versus  $C^*m/\gamma B\tan(\varphi)$  for

Table 1. Test data for 40 vulnerable sites of Guwahati and its adjoining areas.

Location	Latitude and Longitude		Slope Height (m)		Cohesion (kN/m <sup>2</sup> )	Angle of internal friction (°)	Unit weight of the soil (kN/m <sup>3</sup> )	Slope Inclination (°)	Slope Width (m)	Depth of water table	3D-FOS			
	Lat. & Long.	H	H	C							φ	γ	β	B
Jorabat to Umiling	26°05'56.04" N 91°51'44.28" E	38	39.5	30.2	17.6	50	20	30	0.986	0.986	0.986	93.61%	11.06%	4.78%
	26°05'30.04" N 91°51'43.28" E	35	39	30	17.3	50	20	28	1.038	1.038	0.954			
	26°05'20.00" N 91°51'43.00" E	26	38.7	30.5	17.8	60	22	21	0.971	0.971	0.948			
	26°04'31.20" N 91°51'42.10" E	25	39	31.2	17.9	55	20	13	1.010	1.010	1.013			
	26°04'25.20" N 91°51'41.55" E	26	39	30	17.3	50	15	12	1.101	1.101	1.015			
	26°03'44.20" N 91°51'41.32" E	28	39	30	17.3	50	33	12	1.185	1.185	1.066			
	26°03'37.58" N 91°51'41.27" E	29	38.5	30.7	17.5	48	18	10	0.986	0.986	0.995			
	26°03'21.43" N 91°51'41.19" E	29	37.9	30	17.3	45	22	11	1.194	1.194	1.194			
	26°02'55.45" N 91°51'41.03" E	33	38.5	29	17.5	50	17	16	1.123	1.123	1.123			
	26°02'48.56" N 91°51'40.89" E	31	39.2	29.7	17.5	55	30	26	1.210	1.210	1.224			
	26°02'33.16" N 91°51'40.59" E	32	39	30	17.5	50	16	21	1.326	1.326	1.319			
	26°02'17.16" N 91°51'40.40" E	32	39.8	31.3	17.8	45	20	11	1.257	1.257	1.289			
	26°02'11.36" N 91°51'40.37" E	30	39	30	17.3	48	30	23	1.355	1.355	1.332			
	26°02'01.25" N 91°51'40.21" E	32	39	30	17.3	53	17	22	1.289	1.289	1.232			
	26°01'57.25" N 91°51'40.11" E	32	57	39	18	50	26	21	1.260	1.260	1.263			
	26°01'45.25" N 91°51'40.07" E	25	57	39	18	52	30	6	1.700	1.700	1.704			
	26°01'24.55" N 91°51'39.77" E	31	57.2	38.6	18.3	38	16	9	1.934	1.934	1.945			
	26°01'15.43" N 91°51'39.53" E	24	57.5	41.3	19.8	61	24	12	1.543	1.543	1.527			
	26°01'15.00" N 91°51'39.27" E	23	57.5	41.3	19.8	62	25	9	1.680	1.680	1.673			
	26°01'10.00" N 91°51'39.00" E	22	13	41.9	18.5	55	25	13	0.987	0.987	0.967			
26°00'55.25" N 91°51'38.67" E	18	13	41.9	18.7	50	30	8	1.440	1.440	1.438				
26°00'53.45" N 91°51'38.57" E	15	14	42	18.6	65	30	6	1.100	1.100	1.107				
26°00'13.45" N 91°51'38.13" E	17	13.7	42.2	18.5	62	25	7	1.210	1.210	1.179				
26°00'00.45" N 91°51'37.43" E	12	13	41.9	18.5	45	24	4	1.535	1.535	1.533				
25°59'55.45" N 91°51'37.26" E	16	13	41.9	18.5	52	28	5	1.307	1.307	1.301				
25°59'32.45" N 91°51'36.56" E	18	13.5	42	18.5	40	30	9	1.743	1.743	1.604				
25°59'00.24" N 91°51'36.36" E	29	26	42.2	20.4	50	35	18	1.387	1.387	1.273				
25°58'58.24" N 91°51'35.56" E	29	25.5	42	20.5	50	35	18	1.260	1.260	1.266				
25°58'45.24" N 91°51'35.30" E	28	25.5	42.2	20.4	50	36	15	1.093	1.093	1.094				
25°58'24.24" N 91°51'31.32" E	31	25.5	42	20.7	45	20	22	1.110	1.110	1.138				
26°09'02.2" N 91°43'39.7" E	15	15	35	18	60	15	3	1.154	1.154	1.155				
26°09'04.0" N 91°43'41.2" E	18	18	35	17.9	60	54	5	1.016	1.016	1.021				
26°09'06.0" N 91°48'15.9" E	8	35	25	18	65	12	4	1.743	1.743	1.725				
26°09'08.9" N 91°48'13.3" E	11	48	22	18.5	45	16.5	6	2.017	2.017	2.148				
26°11'29.7" N 91°47'24.2" E	10	35	24	18	70	30	2	1.495	1.495	1.492				
26°11'32.2" N 91°47'27.2" E	17	0	37.5	18	45	34	2	1.105	1.105	1.109				
26°11'42.8" N 91°47'53.3" E	20	46	15	18.7	60	80	2	1.047	1.047	1.072				
26°11'37.0" N 91°45'40.7" E	8	36	0	18	50	24	1	1.272	1.272	0.677				
26°12'07.2" N 91°45'58.4" E	15	47.8	0	18	35	30	3	1.020	1.020	0.805				
26°11'47.2" N 91°46'06.0" E	20	27	22	17.8	40	60	6	1.253	1.253	1.212				

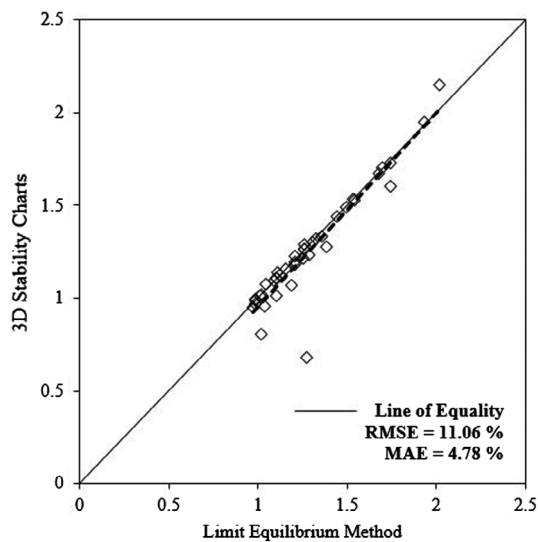


**Figure 14.** Comparison between FOS values obtained from 3D Stability Charts and Limit Equilibrium Method.

width to height ratios (B/H) of the failing slopes ranging from 0.5 to 4.0. Each chart illustrates results of one inclination angle of the slope. The results of slopes of inclination 30 and 35° are shown in Figures 5 and 6 respectively, 40 and 45° are shown in Figures 7 and 8, respectively, 50 and 55° are shown in Figures 9 and 10 respectively, 60 and 65° are shown in Figures 11 and 12 respectively and 70° is shown in Figure 13. Once the B/H values of the mechanism exceed 4.0, the ratio of 3D FOS to 2D FOS approaches to unity ( $\approx 1$ ). However, this ratio exceeds beyond unity ( $>> 1$ ) as the value of B/H lowers to 0.5.

### Case study

A few case studies have been done from Guwahati and its adjoining areas, Assam, India to investigate the extent of vulnerability of these locations. According to a survey, it is found that most of the slopes are either in a damp or wet condition which creates a lot of troubles especially during the monsoons. Massive landslides have occurred resulting too many calamities during the last two decades. Hence, there is a need to check these frequently occurring landslides. In this paper, 40 such vulnerable slopes have been investigated using the 3D limit equilibrium software Slide3 to determine the FOS and a comparison has been made to check the accuracy of the design charts. Table 1 shows the test data for 40 vulnerable sites of Guwahati and its adjoining areas, Assam, India. From Figure 14, it has been found that the FOS obtained from the stability charts are very close to the LEM results. The performance of the stability charts are found to be very good showing a correlation of 93.61%. The error analysis can be performed by computing Root mean squared error (RMSE) and mean absolute error (MAE). The RMSE (0.11) and MAE (0.05) values are found to be very less for outcomes obtained from design charts.

### Conclusion

In this paper, two separate design charts has been presented for 3D slope stability analysis: one for undrained soils where angle of

internal friction,  $\phi_u = 0$  and other for drained soils ( $c - \phi$ ) soils. The use of these charts has been found to be very straight forward. If the slope geometry and hydrological condition is known, the 3D FOS of the slope can be easily computed from the design charts. These charts has been used to calculate the 3D FOS of 40 vulnerable sites from Guwahati and its adjoining areas, Assam, India and the results were compared with the values obtained from LEM. Based on the logical hypothesis (Smith 1986), if a model gives  $R > 0.8$ , and RMSE value is at minimum, there is a strong correlation between the predicted values and measured values. From Table 1, it has been found that the FOS obtained from design charts are having a higher degree of accuracy bearing a correlation of 93.61% and RMSE and MAE of 11.06% and 4.78%, respectively. Hence, the design charts enables to calculate the 3D FOS of the slopes without any iterative procedure. Finally, it can be concluded that the results of this study would be very beneficial in the field of decision-making for the engineers, planners, developers, etc., to estimate the stability for a whole study area using the design charts and create appropriate landslide hazard assessment maps.

### Disclosure statement

No potential conflict of interest was reported by the authors.

### Notes on contributors

**Arunav Chakraborty** is an assistant professor in the Department of Civil Engineering, Tezpur University, Tezpur, Assam. He has been engaged in research activities like Slope Stabilization, Ground Improvement Techniques, Statistical methods and Neural Networks. His most recent article is "Prediction of slope stability using multiple linear regression (MLR) and artificial neural network (ANN)" published in Arabian Journal of Geosciences, Springer. (Arab. J.Geosci. (2017) 10:385; DOI 10.1007/s12517-017-3167-x).

**Diganta Goswami** is a chairman of Indian Geotechnical Society - Guwahati Chapter (NE) and associate professor in the department of Civil Engineering, Assam Engineering College. He has been engaged in research activities in the field of stability of slopes, geotechnical earthquake engineering, environmental geotechniques as well as urban flash flood remediation. He is presently involved in a research project of investigation of deformation modulus and characteristics of soft tertiary rock of Himalayan geology. His most recent article is "Prediction of slope stability using multiple linear regression (MLR) and artificial neural network (ANN)" published in Arabian Journal of Geosciences, Springer. (Arab. J.Geosci. (2017) 10:385; DOI 10.1007/s12517-017-3167-x).

### References

- Anagnosti, P. 1969. "Three Dimensional Stability of Fill Dams." Proceeding of 7th International Conference on Soil Mechanics and Foundation Engineering, Mexico, 275–280.
- Baker, R. 2003. "A Second Look at Taylor's Stability Chart." *Journal of Geotechnical and Geoenvironmental Engineering* 129 (12): 1102–1108.
- Chakraborty, A., and D. Goswami. 2016. "State of the Art: Three Dimensional (3D) Slope Stability Analysis." *International Journal of Geotechnical Engineering* 10 (5): 493–498. doi:10.1080/19386362.2016.1172807.
- Chen, W. F. 1975. *Limit Analysis and Soil Plasticity*. Amsterdam: Elsevier Science.
- Cheng, Y. and Yip, C. (2007). "Three-Dimensional Asymmetrical Slope Stability Analysis Extension of Bishop's, Janbu's, and Morgenstern-Price's Techniques." *Journal of Geotechnical and Geoenvironmental Engineering*, ASCE, 133, (12), 1544–1555.

- Cornforth, D. H. 2005. *Landslides in Practice: Investigation, Analysis, and Remedial/Preventative Options in Soils*. Hoboken, N.J.: Wiley.
- Duncan, J. M. 1996. "State of the Art: Limit Equilibrium and Finite-Element Analysis of Slopes." *Journal of Geotechnical Engineering* 122 (7): 557–596.
- Fredlund, D. G., and J. Krahn. 1978. "Comparison of Slope Stability Methods of Analysis." *Canadian Geotechnical Journal* 14: 429–439.
- Griffiths, D. V., and R. M. Marquez. 2007. "Three-Dimensional Slope Stability Analysis by Elasto-Plastic Finite Elements." *Géotechnique* 57: 537–546.
- Hovland, H. 1977. "Three-Dimensional Slope Stability Analysis Method." *Journal of Geotechnical Engineering Division* 103 (9): 971–986.
- Hungr, O. 1987. "An Extension of Bishop's Simplified Method of Slope Stability Analysis to Three Dimensions." *Géotechnique* 37 (1): 113–117.
- Hungr, O., F. Salgado, and P. Byrne. 1989. "Evaluation of a Three-Dimensional Method of Slope Stability Analysis." *Canadian Geotechnical Journal* 26: 679–686.
- Michalowski, R. L. 2010. "Limit Analysis and Stability Charts for 3D Slope Failures." *Journal of Geotechnical and Geoenvironmental Engineering* 136 (4): 583–593.
- Michalowski, R. L. 2002. "Stability Charts for Uniform Slopes." *Journal of Geotechnical and Geoenvironmental Engineering* 128 (4): 351–355.
- Michalowski, R. L., and A. Drescher. 2009. "Three-Dimensional Stability of Slopes and Excavations." *Géotechnique* 59: 839–850.
- Morgenstern, N., and V. Price. 1965. "The Analysis of the Stability of General Slip Surfaces." *Géotechnique* 15 (1): 79–93.
- Smith, G. N. 1986. *Probability and Statistics in Civil Engineering: An Introduction*. London: Collins.
- Steward, T., N. Sivakugan, S. K. Shukla, and B. M. Das. 2011. "Taylor's Slope Stability Charts Revisited." *International Journal of Geomechanics* 11 (4): 348–352.
- Sun, G., H. Zheng, and W. Jiang. 2011. "A Global Procedure for Evaluating Stability of Three-Dimensional Slopes." *Natural Hazards* 61 (3): 1083–1098.
- Taylor, D. W. 1937. "Stability of Earth Slopes." *Journal of the Boston Society of Civil Engineers* 243: 337–386.
- Ugai, K. (1988). "Three-Dimensional Slope Stability Analysis by Slice Methods." *Proceeding of the International Conference on Numerical Methods in Geomechanics, Innsbruck, Austria, 1369–1374.*